Transmembrane E3 ligase RNF183 mediates ER stress-induced apoptosis by degrading Bcl-xL

Yanfang Wu[a,b,1], Xia Li[a,b,1], Junying Jia[c], Yanpeng Zhang[d], Jing Li[e], Zhengmao Zhu[e], Huaqing Wang[f], Jie Tang[a], and Junjie Hu[a,b,2]

[a]National Laboratory of Biomacromolecules, Chinese Academy of Sciences (CAS) Center for Excellence in Biomacromolecules, Institute of Biophysics, CAS, 100101 Beijing, China; [b]College of Life Sciences, University of CAS, 100101 Beijing, China; [c]Protein Science Core Facility Center, Institute of Biophysics, CAS, 100101 Beijing, China; [d]School of Life Science and Technology, ShanghaiTech University, 201210 Shanghai, China; [e]Department of Genetics and Cell Biology, College of Life Sciences, Nankai University, 300071 Tianjin, China; and [f]Department of Oncology, Institute of Integrative Oncology, Tianjin Union Medical Center, 300121 Tianjin, China

Edited by Peter Walter, University of California, San Francisco, CA, and approved February 15, 2018 (received for review September 18, 2017)

The accumulation of misfolded proteins in the endoplasmic reticulum (ER) causes ER stress and triggers the unfolded protein response (UPR). Failure to resolve ER stress leads to apoptotic cell death via a yet unclear mechanism. Here, we show that RNF183, a membrane-spanning RING finger protein, localizes to the ER and exhibits classic E3 ligase activities. Sustained ER stress induced by different treatments increases RNF183 protein levels posttranscriptionally in an IRE1α-dependent manner. Activated IRE1 reduces the level of miR-7, which increases the stability of RNF183 transcripts. In addition, overexpression of RNF183 leads to increased apoptosis and its depletion alleviates ER stress-induced apoptosis. Furthermore, RNF183 interacts with Bcl-xL, an antiapoptotic member of the Bcl-2 family, and polyubiquitinates Bcl-xL for degradation. Thus, RNF183 plays an important role in executing programmed cell death upon prolonged ER stress, likely by inducing apoptosis through Bcl-xL.

RING finger protein | endoplasmic reticulum stress | unfolded protein response | apoptosis | Bcl-xL

The endoplasmic reticulum (ER) handles the synthesis of secretory proteins, endomembrane proteins, and most integral membrane proteins. When protein folding errors occur in the ER, the misfolded products are eliminated by the ER-associated degradation (ERAD) pathway (1, 2). If substantial amounts of misfolded proteins accumulate, the ER will enter a stressed state, triggering a series of signaling events known as the unfolded protein response (UPR) (3, 4). In higher eukaryotes, the UPR system consists of three well-characterized signaling arms. IRE1α, a membrane-spanning kinase and endoribonuclease, splices XBP1 mRNA, which subsequently activates a stress-regulating transcription program (5, 6). PERK, another membrane-spanning kinase, mainly phosphorylates eIF2α, inhibiting translation and alleviating ER burden (7). Activated PERK also induces transcription factors, such as ATF4 and CHOP, for further ER stress responses (8, 9). ATF6, a transmembrane transcription factor, is transported to the Golgi and cleaved into a soluble form that regulates the expression of a subset of UPR-responsive genes (10).

Upon stress, the ER initially attempts to restore its homeostasis via UPR signaling. However, if the stress is sustained, apoptotic cell death will be triggered through UPR pathways (11). In pathological conditions in which prolonged ER stress occurs, it may be beneficial to prevent excess apoptosis, especially for cells that are difficult to regenerate. Thus, inhibition of ER stress-induced apoptosis would be a valuable therapeutic strategy. However, the mechanism of UPR-induced apoptosis is not entirely clear. Involvement of the activation of stress-responsive kinase JNK or transcriptional regulation of Bcl-2 family proteins has been implicated (12–15). In addition, death receptor 5 (DR5) can be up-regulated by the UPR to control apoptosis (16), and caspase-2 can be derepressed by IRE1-dependent microRNA (miR) decay (17). Therefore, multiple pathways must exist to execute apoptosis upon prolonged ER stress.

Results

Apoptosis-Promoting RNF183 Localizes to the ER. In an effort to identify apoptosis-promoting RING finger proteins (RNFs), we found that overexpression of RNF183 increases apoptosis (Fig. 1*A*) and reduces cell survival (*SI Appendix*, Fig. S1). Primary sequence analysis using PredictProtein (18) revealed that human RNF183 contains an N-terminal RING-type zinc finger (residues 13–60) and a C-terminal transmembrane domain (Fig. 1*B*). RNF183 transcripts were ubiquitous (*SI Appendix*, Fig. S2*A*) and more abundant in mouse kidney and lung tissues (*SI Appendix*, Fig. S2*B*). GFP-tagged RNF183 transfected into COS-7 cells mainly localized to the ER and Golgi and was not found in mitochondria (Fig. 1*C*). Because commercially available or in-house antibodies failed to specifically recognize endogenous RNF183 protein, we generated a GFP-tag knockin cell line for further analysis (*SI Appendix*, Fig. S2*C*). Coding sequences for an N-terminal GFP were inserted into the genomic locus of RNF183 in HeLa cells using the CRISPR/Cas9 system (19, 20). Single clones of knockin cells were selected by fluorescent activated cell sorting (FACS) (*SI Appendix*, Fig. S2*D*) and confirmed by PCR (*SI Appendix*, Fig. S2*E*) and immunoblotting (*SI Appendix*, Fig. S2*F*). We chose one of the clones, termed KI-A6, for subsequent experiments. Fluorescent imaging of the KI-A6 cells

Significance

The accumulation of unfolded proteins in the endoplasmic reticulum (ER) is a pathological condition observed in many diseases, including cancer, diabetes, and neurodegenerative diseases. Failure to relieve the cellular stress via adaptive mechanisms of the unfolded protein response (UPR) activates apoptotic cell death. We demonstrate that a membrane-anchored RING finger protein, RNF183, is specifically induced by prolonged ER stress. RNF183 is regulated by IRE1, mainly through miR-7. As an E3 ligase, RNF183 ubiquitinates Bcl-xL, causing its degradation and subsequent apoptosis. Our findings imply that manipulation of RNF183 activity may help control cell fate in pathological conditions and suggest that the close contact between the ER and mitochondria plays a key role in cellular signaling.

Author contributions: Y.W., X.L., J.T., and J.H. designed research; Y.W., X.L., J.J., Y.Z., and J.L. performed research; Y.W., X.L., J.J., Z.Z., H.W., and J.H. analyzed data; and J.H. wrote the paper.

The authors declare no conflict of interest.

This article is a PNAS Direct Submission.

[1]Y.W. and X.L. contributed equally to this work.

[2]To whom correspondence should be addressed. Email: huj@ibp.ac.cn.

This article contains supporting information online at www.pnas.org/lookup/suppl/doi:10.1073/pnas.1716439115/-/DCSupplemental.

Published online March 5, 2018.

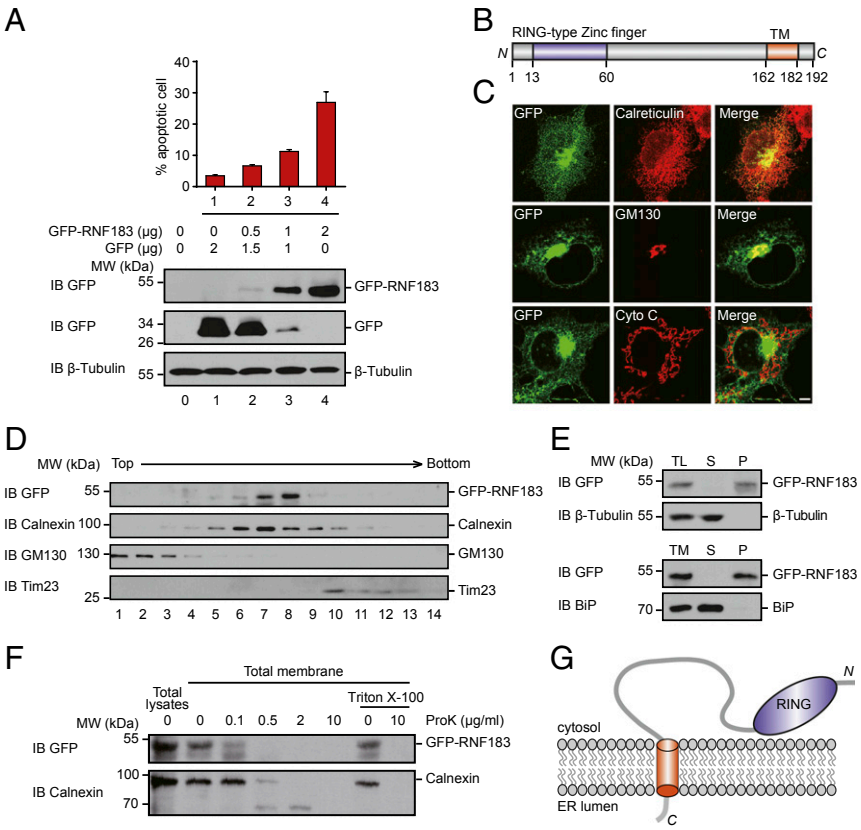

Fig. 1. RNF183 is an ER-localized membrane protein that regulates apoptosis. (*A*) HeLa cells were transfected with GFP and GFP-tagged RNF183 as indicated. Apoptosis was measured by Annexin-V-PE/7-AAD staining and analyzed by FACS. (*Top*) Percentages of Annexin-V-positive cells. Error bars indicate the SEM. (*Bottom*) Immunoblotting (IB) of GFP and GFP-RNF183. β-Tubulin was used as a loading control. (*B*) Schematic representation of the predicted domain structure of RNF183. Amino acid numbers are shown. (*C*) HeLa cells expressing GFP-tagged RNF183 were fixed, permeabilized, and immunostained with anti-calreticulin, GM130, and cytochrome C antibodies. (Scale bar: 10 μm.) (*D*) Cell fractionation of KI-A6-HeLa cells (see *SI Appendix*, Fig. S2 for details). The total lysates (TL) were separated on a 30% Percoll gradient and the fractions subjected to IB. Calnexin, ER marker; Tim23, mitochondrial marker; GM130, Golgi marker. (*E*) The TL of KI-A6-HeLa cells were separated into soluble (S) and pelleted membrane (P) fractions and then immunoblotted for GFP or the cytosolic protein β-tubulin. The total membrane (TM) fractions were alkaline extracted and S and P fractions immunoblotted for GFP and the soluble protein BiP. (*F*) The lysates of KI-A6-HeLa cells were digested with proteinase K in the presence or absence of Triton X-100, followed by IB. Membrane-spanning ER protein calnexin was used for comparison. (*G*) Topological diagram of RNF183. MW, molecular weight (in all figures).

revealed very weak GFP signals, suggesting a low abundance of endogenous RNF183. Cell fractionation using a Percoll gradient resulted in RNF183 comigrating with ER marker calnexin, separate from Golgi marker GM130 (Fig. 1*D*). These results suggest that RNF183 localizes to the ER and can overflow into the Golgi upon overexpression.

We also performed membrane sedimentation and alkaline extraction to investigate whether RNF183 integrates into ER membranes. Endogenous GFP-RNF183 precipitated with membrane fractions and remained in membranes upon alkaline treatment (Fig. 1*E*). The GFP tag was susceptible to proteinase K digestion in microsomes or Triton-solubilized lysates (Fig. 1*F*). Taken together, these data suggest that RNF183 is an integral membrane protein with an N terminus, including the predicted RING finger domain, exposed to the cytosol (Fig. 1*G*). Such topology suggests that RNF183 may be a tail-anchored protein.

RNF183 Is Induced by Prolonged ER Stress. Next, we investigated whether ER-localized RNF183 is involved in the regulation of ER stress, and possibly stress-induced apoptosis. When GFP-RNF183 knockin cells were treated with thapsigargin (Tg), an inhibitor of the SERCA calcium pump commonly used to trigger the UPR, RNF183 was significantly up-regulated after 24 h, at which point apoptosis was activated, as indicated by the cleavage of polyADP ribose polymerase (PARP) (Fig. 2*A*). The induction of RNF183 was maintained at 36 h, when apoptosis was more prominent (Fig. 2*A*). The same delayed induction was observed with several other known inducers of the UPR, including tunicamycin (Tm) (Fig. 2*B*), DTT, and palmitic acid (PA) (*SI Appendix*, Fig. S3*A*). In contrast, staurosporine or etoposide, apoptotic stressors that do not affect ER stress, did not activate RNF183; instead, treatment with these drugs reduced the levels of RNF183, even when apoptosis was clearly triggered (i.e., PARP cleavage) (*SI Appendix*, Fig. S3*B*). The role of RNF183 in prolonged ER stress was further confirmed when GFP-RNF183 was depleted using siRNA in the knockin cells. Prolonged treatment with Tg (Fig. 2*C*) or Tm (Fig. 2*D*) caused an increase in apoptotic cells, but this increase was partially reversed upon RNF183 depletion (Fig. 2*E*).

The induction of RNF183 is less likely caused by transcriptional regulation, because RNF183 transcripts were mostly unchanged during Tm treatment and only increased at late time points (Fig. 2*F*). To investigate whether RNF183 is regulated transcriptionally, we generated an Flp-In-293 cell line expressing Myc-RNF183 (*SI Appendix*, Fig. S4*A*). Transcription of Myc-RNF183 was controlled by the addition of tetracycline, which resulted in a much higher level of transcripts than what is expected from endogenous transcription (*SI Appendix*, Fig. S4*B*) and the protein expression. When the cells were treated with both tetracycline and Tm, further induction of Myc-RNF183 occurred

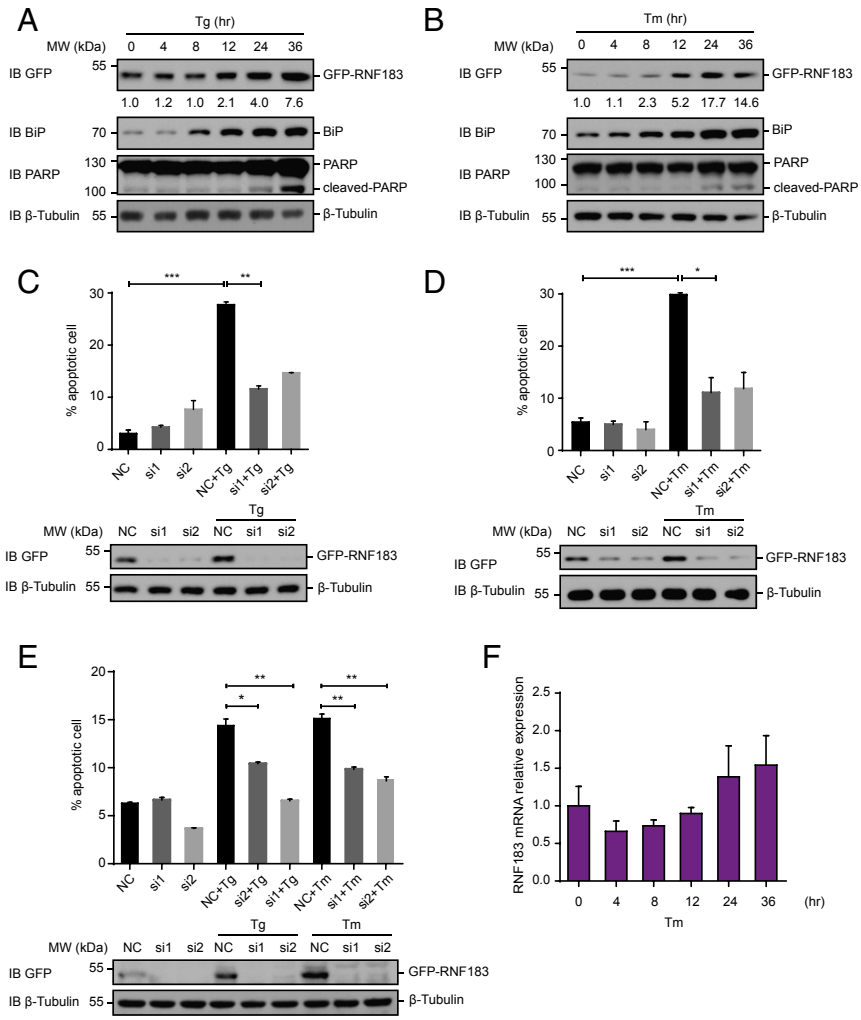

Fig. 2. RNF183 is induced by prolonged ER stress. (*A*) KI-A6-HeLa cells were treated with 5 μM thapsigargin (Tg) for varying duration. The levels of GFP-RNF183, BiP, and PARP were analyzed by immunoblotting (IB). β-Tubulin was used as a loading control. The relative levels of RNF183 were quantified using the Gel-Pro analyzer software. (*B*) As in *A*, but with 10 μg/mL tunicamycin (Tm). (*C* and *D*) KI-A6-HeLa cells were transfected with control siRNA (NC) or two siRNAs against RNF183 (100 nM each, si1 and si2) and treated with Tg (*C*) or Tm (*D*) for another 36 h. The apoptosis ratio was determined by Annexin V-FITC/PI staining. Quantified data represent mean ± SEM. $*P < 0.05$, $**P < 0.01$, $***P < 0.001$, *t* test. Levels of GFP-RNF183 were determined by IB using GFP antibodies, with GAPDH as a loading control. (*E*) As in *C* and *D*, but treated with Tg or Tm for another 24 h. (*F*) Quantitative RT-PCR analysis of RNF183 in HeLa cells after treatment with vehicle, 10 μg/mL Tm at varying time points. RNA expression levels are fold change of the target gene normalized to GAPDH. Graphs depict means ± SD of triplicates.

after 24 h without much change in the transcript level (*SI Appendix*, Fig. S4*C*). UPR-dependent augmentation of Myc-RNF183 was also observed with other ER stress-inducing treatments (*SI Appendix*, Fig. S4*D*). Taken together, the results indicate that prolonged ER stress regulates RNF183 likely more at protein levels posttranscriptionally.

RNF183 Is Regulated by the IRE1 Pathway. To determine which UPR pathway is involved in RNF183 activation, we used specific inhibitors targeting individual signaling arms. Inhibition of PERK by integrated stress response inhibitor (ISRIB) (21), while blocking induction of its target gene *CHOP* (*SI Appendix*, Fig. S4*E*), did not prevent a UPR-dependent increase of RNF183 in Flp-In-293 cells. In contrast, when the inhibitor of the nuclease of IRE1α, 4μ8C, was used, XBP-1 splicing and the Tm-dependent induction of RNF183 were prevented (*SI Appendix*, Fig. S4*F*). The same results were obtained when GFP-RNF183 knockin cells were treated with 4μ8C/Tm (Fig. 3*A*) or 4μ8C/Tg (Fig. 3*B*). Furthermore, when IRE1α-HA was transfected into Myc-RNF183 Flp-In-293 cells (*SI Appendix*, Fig. S5*A*) or KI-A6-HeLa cells (*SI Appendix*, Fig. S5*B*), RNF183 accumulated even in the absence of ER stress. Conversely, when IRE1α was depleted using siRNAs, RNF183 was no longer induced by ER stress (*SI Appendix*, Fig. S5*C*). These results indicate that RNF183 is regulated by IRE1α signaling.

Activated IRE1α splices the XBP1 transcript, resulting in a transcriptionally potent form of Xbp1. However, the induction of RNF183 occurred only after prolonged UPR activation, during which XBP1 splicing by IRE1α was largely diminished (Fig. 3*C*). Consistently, prolonged inhibition of IRE1α by 4μ8C was necessary to prevent RNF183 induction (Fig. 3*D*). In addition, ectopic expression of spliced Xbp1 failed to augment RNF183 (*SI Appendix*, Fig. S5 *D* and *E*), and depletion of XBP1 had no impact on RNF183 induction upon ER stress (*SI Appendix*, Fig. S5*F*). These results suggest that RNF183 induction is independent of XBP1 splicing by IRE1α.

RNF183 Is Regulated Through miR-7. As activated IRE1α degrades mRNA or miR for UPR adaptation (22), we tested whether miR is involved in regulating the levels of RNF183. When mimics of several miRs were transfected into KI-A6 cells, miR-7 caused a significant reduction of RNF183, and miR-96 and -34a caused mild

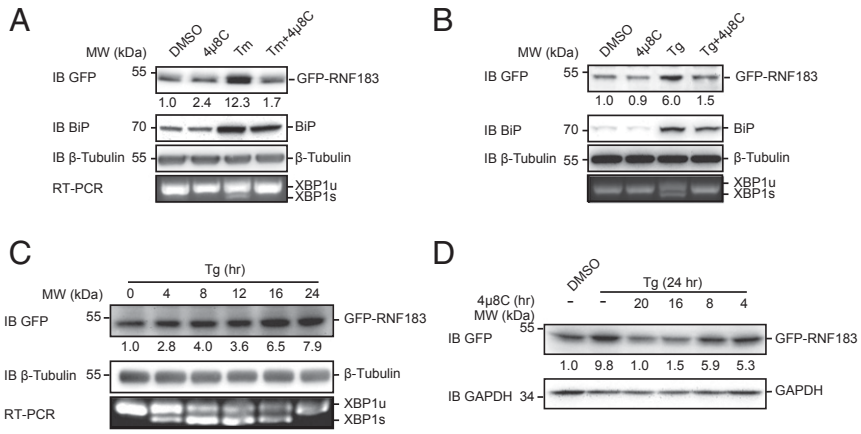

Fig. 3. RNF is regulated by the IRE1 pathway. (*A*) KI-A6 cells were treated with Tm (10 μg/mL) or IRE1 inhibitor 4μ8C (50 μM) as indicated. The levels of RNF183, BiP, and PARP were analyzed by IB. β-Tubulin was used a loading control. Unspliced XBP1 (XBP1u) and spliced XBP1 (XBP1s) were amplified by RT-PCR and separated on an agarose gel. RNF183 protein level quantification was performed using the Gel-Pro analyzer software. (*B*) As in *A*, but with Tg (5 μM). (*C*) KI-A6-HeLa cells were treated with Tg (5 μM) for varying duration. The levels of GFP-RNF183 were analyzed by immunoblotting (IB) with β-tubulin being a loading control. XBP1u and XBP1s were amplified by RT-PCR and separated on an agarose gel. RNF183 protein level quantification was performed using the Gel-Pro analyzer software. (*D*) KI-A6-HeLa cells were treated with DMSO or Tg (5 μM) for 24 h, during which 4μ8C (50 μM) was added for indicated duration toward the end of Tg treatment. The levels of GFP-RNF183 were analyzed by IB. GAPDH was used a loading control. RNF183 protein level quantification was performed using the Gel-Pro analyzer software.

effects (Fig. 4*A*). Treatment with miR-7 inhibitor resulted in the accumulation of RNF183 in KI-A6 cells, but miR-17 inhibitor had a much weaker effect (Fig. 4*B*). Similarly, mimics of miR-7 and -96, but not -34a and other miRs, decreased the RNF183 levels in Flp-In-293 cells (*SI Appendix*, Fig. S6*A*), and inhibitor of miR-7, but not miR-17 or -96, decreased the RNF183 levels in these cells (*SI Appendix*, Fig. S6*B*). These results indicate that RNF183 is mainly negatively regulated by miR-7.

To further investigate whether miR-7 is controlled by the IRE1 pathway, we measured the expression of miR-7 upon prolonged ER stress. Consistent with our prediction, the levels of miR-7 gradually decreased (Fig. 4*C* and *SI Appendix*, Fig. S6*C*) during ER stress and overexpression of IRE1α alone was sufficient to eliminate miR-7 (*SI Appendix*, Fig. S6 *D* and *E*). Furthermore, depletion of IRE1α blocked ER stress-dependent miR-7 down-regulation (*SI Appendix*, Fig. S6*G*), whereas depletion of XBP1 had no effect (*SI Appendix*, Fig. S6*H*). Furthermore, miR-7 reduction correlated with an increase in RNF183 (Fig. 3*C*) and could be reversed by treatment with 4μ8C (Fig. 4*D* and *SI Appendix*, Fig. S6*F*). These results suggest that IRE1α reduces miR-7 levels, which then likely induces RNF183.

miR usually regulates mRNA stability or translational efficiency. When miR-7 was transfected into KI-A6 cells, RNF183 transcript was decreased (Fig. 4*E*). Conversely, when miR-7 was decreased after prolonged Tg exposure, RNF183 transcript was increased, which was again susceptible to 4μ8C (Fig. 4*F*). These results suggest that miR-7 likely functions in destabilizing RNF183 mRNA.

We analyzed the 3′-UTR of RNF183 and found binding sites for both miR-7 and -96 (*SI Appendix*, Fig. S7*A*). To probe the role of the RNF183 3′-UTR, we generated Myc-RNF183 Flp-In-293 cells with or without its 3′-UTR (*SI Appendix*, Fig. S4*A*). Removal of the 3′-UTR caused a dramatic decrease in the RNF183 protein level and a failure of transcript stabilization during Tm treatment (Fig. 4*G*). To directly test the role of the RNF183 3′-UTR, we fused it to the coding sequence of luciferase. Overexpression of miR-7 mimic, but not miR-17, directly affected luciferase activities when the RNF183 3′-UTR was attached (*SI Appendix*, Fig. S7*B*). The reduction was diminished when the miR-7 binding site in the 3′-UTR was mutated (*SI Appendix*, Fig. S7*C*). These results suggest the targeting of miR-7 at the 3′-UTR of RNF183.

RNF183 Is an E3 Ligase. The RING domain of RNF183 possesses a classical C_3HC_4 motif (Fig. 5*A*) that can bind two zinc ions. Such a domain often plays a key role in the ubiquitination pathway, serving as part of the E3 ligase (23). The E3 ligase activity of RNF183 was suggested previously (24, 25). Consistently, overexpression of RNF183 resulted in self-ubiquitination (Fig. 5*B*) and an accumulation of ubiquitinated proteins in cells (Fig. 5*C*) when the proteasome was inhibited by MG132. Furthermore, purified cytosolic segment RNF183 (cytRNF183), when supplied with an E1 (UBA1), a promiscuous E2 (UBCU5C), ubiquitin (Ub), and ATP, was able to ubiquitinate itself (Fig. 5*D*). As expected, the ubiquitination activity was lost when the two cysteines (C13/C15) in the zinc fingers were mutated to serines (Fig. 5*D*). Therefore, RNF183 is an active E3 ligase.

RNF183 Ubiquitinates Bcl-xL. Given that RNF183 promotes apoptosis, we speculated that it might target an antiapoptotic factor for degradation. Several HA-tagged antiapoptotic Bcl-2 family members, including Bcl-2, Bcl-xL, BAX, and BAD, were individually coexpressed with GFP-RNF183 in HeLa cells and the cell extracts subjected to immunoprecipitation. GFP antibodies precipitated HA-Bcl-xL (Fig. 6*A*) but not other antiapoptotic factors (*SI Appendix*, Fig. S8*A*). Conversely, in cells expressing HA-Bcl-xL, HA antibodies were able to precipitate GFP-RNF183 (Fig. 6*B*). Importantly, when endogenous RNF183 in KI-A6 cells was precipitated by anti-GFP antibodies, endogenous Bcl-xL coprecipitated (Fig. 6*C*). Purified GST-tagged Myc-RNF183, when pulled down by glutathione agarose, precipitated purified Bcl-xL-HA (Fig. 6*D*). Less Bcl-2-HA coprecipitated under the same conditions (*SI Appendix*, Fig. S8*B*). No interaction was detected when GST-Myc was used (Fig. 6*D*). Finally, when the purified cytosolic domains of RNF183 and Bcl-xL were mixed, Bcl-xL coprecipitated with RNF183 (Fig. 6*E* and *SI Appendix*, Fig. S8*C*). Similar results were obtained using lysates from cells coexpressing the GFP-tagged cytosolic domain of RNF183 and HA-Bcl-xL (Fig. 6*F*). These data suggest that RNF183 interacts directly with Bcl-xL, likely through their cytosolic domains.

Next, we investigated whether Bcl-xL is ubiquitinated by RNF183 and subsequently degraded. Myc-tagged Ub and HA-tagged Bcl-xL were coexpressed with GFP or GFP-RNF183 in HeLa cells. Upon immunoprecipitation of Bcl-xL with HA antibodies, the ubiquitination level was assessed by anti-Myc immunoblotting. The

CELL BIOLOGY

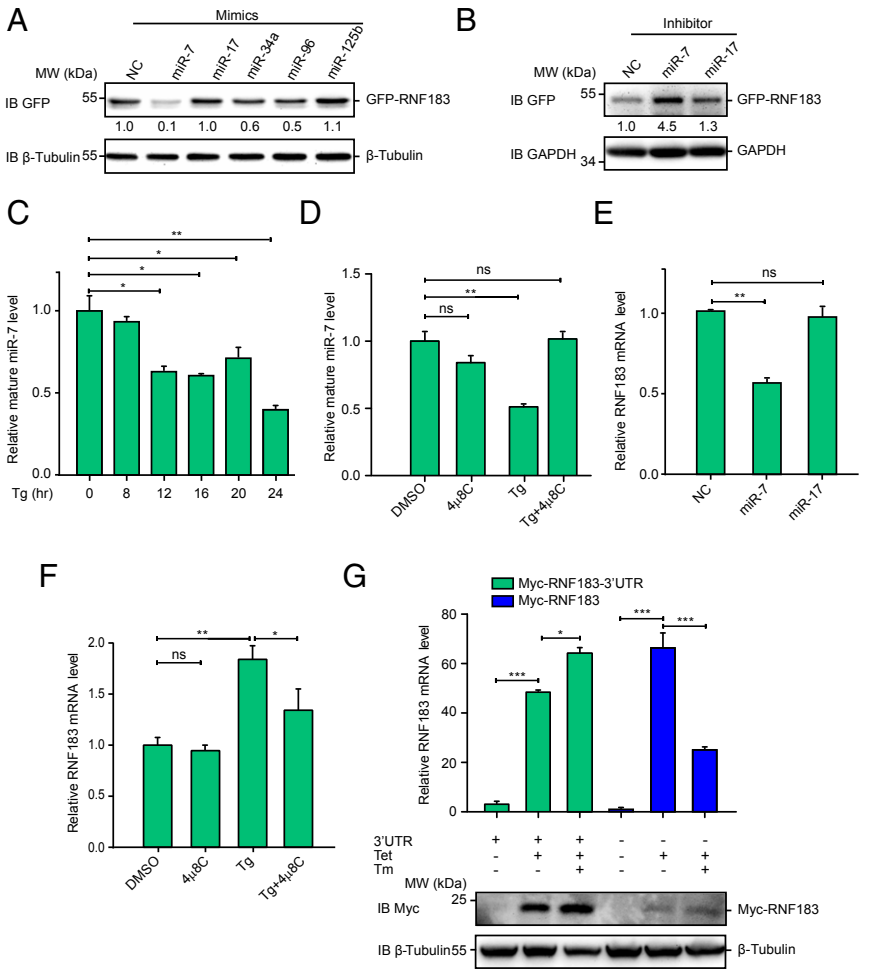

Fig. 4. RNF183 is negatively regulated by miR-7. (*A*) Several miR mimics were transfected into KI-A6-HeLa cells for 24 h, and IB of GFP-RNF183 was performed. GAPDH was used as a loading control. RNF183 protein level quantification was performed using the Gel-Pro analyzer software. (*B*) Nonspecific miR control (NC), miR-7, and miR-17 inhibitors were transfected into KI-A6-HeLa cells for 24 h. Levels of GFP-RNF183 were analyzed by IB using GFP antibodies, with GAPDH as a loading control. RNF183 protein level quantification was performed using the Gel-Pro analyzer software. (*C*) KI-A6-HeLa cells were treated with Tg (5 μM) for indicated time. Mature miR-7 expression levels were determined by qPCR. Quantified data represent mean ± SEM. $*P < 0.05$, $**P < 0.01$, *t* test. (*D*) Flp-in-293 Myc-RNF183 cells were treated with DMSO, Tg, or 4μ8C as indicated. Mature miR-7 expression levels were determined by qPCR. Quantified data represent mean ± SEM. $**P < 0.01$; ns, no significant difference; *t* test. (*E*) NC, miR-7, or miR17 mimics was transfected into KI-A6-HeLa cells for 24 h. Relative RNF183 mRNA levels were determined by qPCR. Quantified data represent mean ± SEM. $**P < 0.01$; ns, no significant difference; *t* test. (*F*) KI-A6-HeLa cells were treated with DMSO, Tg, or 4μ8C as indicated. Relative RNF183 mRNA levels were determined by qPCR. Quantified data represent mean ± SEM. $*P < 0.05$, $**P < 0.01$; ns, no significant difference; *t* test. (*G*) Flp-in-293 Myc-RNF183 and Myc-RNF183-3′-UTR cells were treated with/without tetracycline (Tet), or with/without Tm as indicated. RNF183 transcript levels were analyzed by qPCR. (*Top*) Relative RNF183 mRNA levels. (*Bottom*) IB of Myc-RNF183; β-tubulin was used as a loading control. Quantified data represent mean ± SEM. $*P < 0.05$, $**P < 0.01$, $***P < 0.001$, *t* test.

presence of GFP-RNF183, but not GFP, caused polyubiquitination of Bcl-xL (Fig. 7*A*). This modification was dramatically reduced when the RING finger of RNF183 was mutated or the transmembrane domain deleted (ΔTM) (Fig. 7*A*). The dependence of RNF183-TM implies that the E2 for RNF183 is likely ER anchored. In contrast, Bcl-xL ubiquitination was not affected when RNF183 self-ubiquitination was eliminated by substituting all lysine residues with arginines (Fig. 7*A*). We then tested this reaction using purified components in vitro. RNF183 ubiquitinated Bcl-xL but failed to modify Bcl-2 (Fig. 7*B*). These results indicate that Bcl-xL is a substrate of RNF183.

RNF183 Targets Bcl-xL for Degradation upon Prolonged ER Stress. Ub linkage on different lysine residues leads to different destinies for the modified substrate (26). To investigate the type of ubiquitination RNF183 induces with Bcl-xL, three mutated Ub-Myc molecules (K29R, K48R, and K63R) were individually cotransfected with Bcl-xL-HA and RNF183-Flag into HeLa cells. Polyubiquitination of Bcl-xL was blocked by K29R and K48R, but not K63R (*SI Appendix*, Fig. S9*A*), suggesting that ubiquitinated Bcl-xL-HA is targeted for proteasomal degradation. Consistently, increasing amounts of RNF183-HA reduced the level of Bcl-xL-Flag in HeLa cells (*SI Appendix*, Fig. S9*B*), and the RNF183-dependent loss of Bcl-xL was prevented if proteasome inhibitor MG132 was added (*SI Appendix*, Fig. S9 *C* and *D*). Induction of Myc-RNF183 by tetracycline in Flp-In-293 cells had little effect on Bcl-xL, whereas additional transfection of Myc-RNF183, which boosted level of RNF183 equivalent to what was induced by Tm treatment, caused apparent decreases of Bcl-xL (*SI Appendix*, Fig. S9*E*). To confirm that Bcl-xL levels play an important role in ER stress-induced apoptosis, we overexpressed Bcl-xL in HeLa cells subjected to ER stress. As expected, increased levels of Bcl-xL protected cells from apoptosis under conditions of prolonged ER stress (*SI Appendix*, Fig. S10*A*).

Next, we examined whether endogenous Bcl-xL is also ubiquitinated and degraded during prolonged ER stress in an

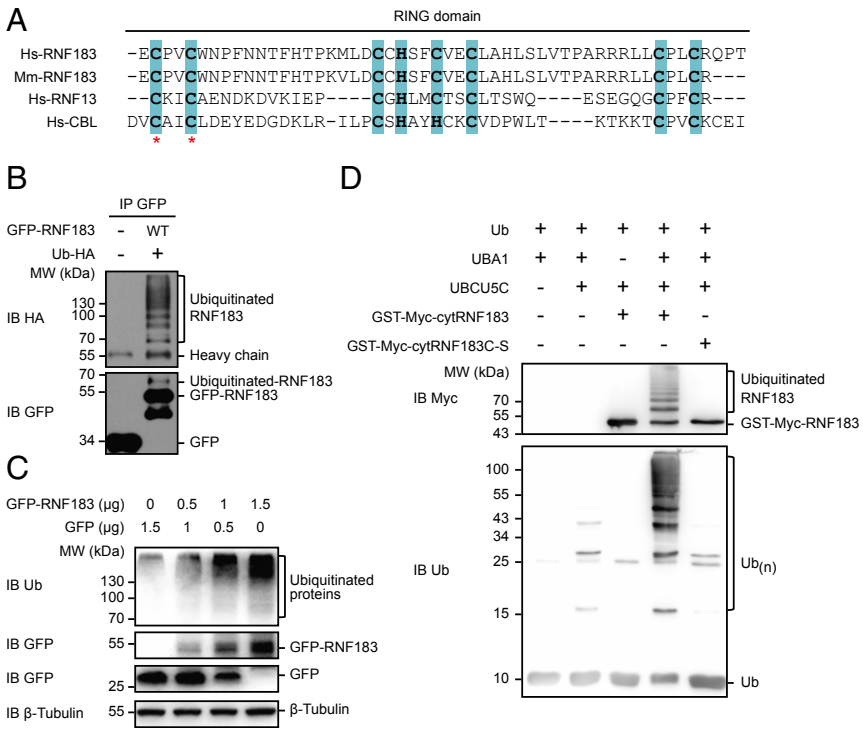

Fig. 5. RNF183 is an E3 ligase. (*A*) Sequence alignment of RING finger domains. The conserved C_3HC_4 motif is highlighted in bold with a blue background. The red asterisks (*) indicate the two mutated cysteines in RNF183. Hs, *Homo sapiens*; Mm, *Mus musculus*. (*B*) GFP-RNF183 and Ub-HA were cotransfected into HeLa cells. RNF183 was precipitated using anti-GFP antibodies and its ubiquitination analyzed by immunoblotting using the indicated antibodies. (*C*) GFP or GFP-tagged RNF183 were transfected into HeLa cells at the indicated concentrations for 24 h and total ubiquitinated proteins analyzed with anti-Ub antibodies. (*D*) Purified recombinant GST-Myc-cytRNF183 (residues 1–161) or RING finger mutant (CS, C13S/C15S) were incubated at 37 °C for 1 h in the presence or absence of E1 (UBA1), E2 (UBCU5C), Ub, and ATP. Samples were subjected to immunoblotting using anti-Myc and anti-Ub antibodies.

RNF183-dependent manner. When GFP-RNF183 knockin cells were treated with Tg or Tm, the level of endogenous Bcl-xL decreased, correlating with the increase in GFP-RNF183 and the cleavage of apoptotic marker PARP (Fig. 7*C*). The loss of Bcl-xL was most prominent when RNF183 induction by ER stress was substantial and apoptosis detectable (*SI Appendix*, Fig. S10*B*), and is less likely due to transcriptional regulation, as Bcl-xL transcripts increased under the tested conditions (*SI Appendix*, Fig. S10*C*). The ubiquitination of endogenous Bcl-xL, assessed under denatured conditions, also reached a maximum level when ER stress was induced for 24 h, accompanied by a drastic increase in the level of GFP-RNF183 and the cleavage of PARP (Fig. 7*E* and *SI Appendix*, Fig. S10*D*). Finally, when endogenous GFP-RNF183 was depleted using siRNA during sustained ER stress, ubiquitination and degradation of Bcl-xL was inhibited and apoptosis decreased (Fig. 7 *D* and *F* and *SI Appendix*, Fig. S10 *E* and *F*). Collectively, these results confirm that RNF183 is responsible for Bcl-xL ubiquitination and degradation during prolonged ER stress.

Discussion

Our results suggest how ER-localized E3 ligase RNF183 triggers apoptosis in response to prolonged ER stress. During extended treatment with UPR-inducing reagents, activated IRE1α caused a slow accumulation of RNF183 protein, likely through miR-7 and miR-96. Elevated levels of RNF183 promote its binding to Bcl-xL, polyubiquitination, and subsequent proteasomal degradation. The progressive decrease in Bcl-xL levels eventually induces the intrinsic apoptotic pathway.

The induction of RNF183 during ER stress is less likely through transcriptional activation. Upon IRE1α activation, miR-7 readily decayed, likely by the digestion of miR precursors through the IRE1-dependent decay of mRNA (RIDD) (17, 27). Even though XBP1 splicing by IRE1 is gradually turned off during the course of ER stress (28), the RIDD activity likely lasts longer. Decreased occupancy of miR-7 at the RNF183 3′-UTR eventually stabilizes the RNF183 mRNA and leads to increased protein levels. The regulation of RNF183 by miR-7 has been confirmed independently (25). Furthermore, it is likely that miR-96, which is known to be down-regulated by RIDD, may also be involved by binding to the 3′-UTR of RNF183. Whether additional UPR-related mechanisms of RNF183 induction, such as post-translational modification and increase of protein stability/activity, are involved, remains to be investigated. The fine-tuned timing of RNF183 induction is reminiscent of DR5 in UPR-triggered apoptosis, both of which fit their role in prolonged ER stress.

Bcl-xL is usually localized to the mitochondria, whereas RNF183 is anchored to the ER. Some Bcl-xL may be targeted to the ER (29, 30) and accessed by RNF183 directly. Because their cytosolic domains can interact with each other, it is also feasible that full-length molecules engage under physiological conditions, even without sitting in the same membrane. Mitochondria and the ER frequently come into close proximity to form membrane contact sites (31, 32), which would promote RNF183–Bcl-xL interactions. In a similar case, cytosolic substrate, when anchored on the outer mitochondrial membrane, can be efficiently modified by an ER-bound E3 ligase (33).

As the most outreaching organelle, tubular ER potentially senses a variety of stresses (34). Therefore, ER-orchestrated apoptosis is an emerging theme during the cellular stress response. In addition to RNF183, by which antiapoptotic factor Bcl-xL is targeted to trigger apoptosis, ERAD component gp78 controls the stability of apoptotic effector BOK, a noncanonical member of the Bcl-2 family (35); when ER homeostasis is disrupted, subsequent ERAD inhibition could also initiate apoptosis by accumulating BOK.

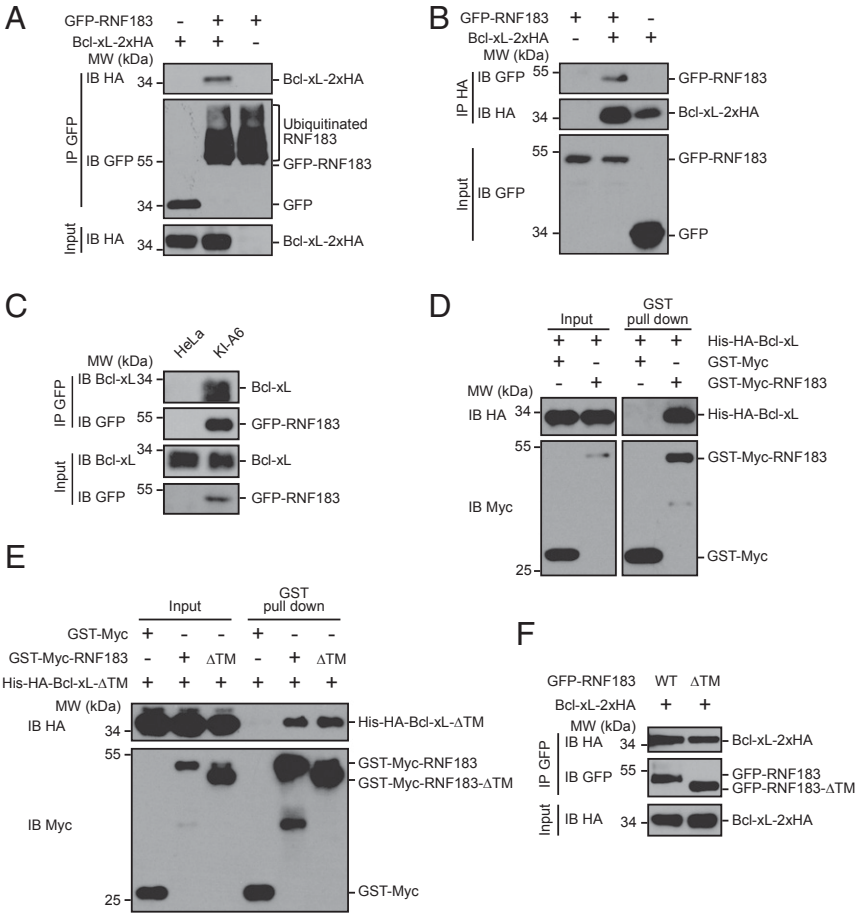

Fig. 6. RNF183 interacts with Bcl-xL. (*A*) GFP-RNF183 and Bcl-xL-2xHA were cotransfected into HeLa cells and the cell lysates precipitated using anti-GFP or anti-HA antibodies. Immunoblotting was carried out using the indicated antibodies. (*B*) As in *A*, for reciprocal IP. (*C*) Lysates from HeLa or KI-A6-HeLa cells were immunoprecipitated by anti-GFP antibodies and immunoblotted with anti-Bcl-xL and GFP antibodies. (*D*) Recombinant GST-Myc or GST-Myc-RNF183 was incubated with His-HA-Bcl-xL. The mixtures were precipitated with glutathione beads, followed by IB with anti-Myc and HA antibodies. (*E*) As in *D*, but with the indicated constructs. (*F*) As in *A*, but with the indicated constructs.

The endogenous level of RNF183 in HeLa cells is very low. In mouse tissues, it is most abundant in the testes and kidneys and may play a role in regulating apoptosis there. RNF183 has been shown to associate with one of the cancer–testis antigens (CTAs) FATE1, and likely targets BCL2-interacting killer (BIK) for degradation (24). RNF183 was also recently implicated in the regulation of inflammatory bowel disease and colorectal cancer (25, 36), suggesting additional functions and substrates.

Materials and Methods

Cell Culture and Treatment. HeLa, KI-A6, and COS-7 cells were cultured in DMEM (Invitrogen) supplemented with 10% (vol/vol) FBS, 100 units/mL penicillin, and 50 μg/mL streptomycin at 37 °C in a 5% CO_2 humidified incubator. For Flp-in 293T cells, 2 mM L-glutamine, 100 μg/mL zeocin, and 15 μg/mL blasticidin were added. Hygromycin B (100 μg/mL) replaced zeocin in Myc-RNF183-Flip-in 293T cells. The cells were maintained in a logarithmic growth phase and seeded at an appropriate number 24 h before treatment. According to the manual, monolayer cells were transfected at 70–90% confluence using TurboFect Transfection Reagent (Thermo Fisher Scientific) for plasmids and Lipofectamine RNAiMAX Transfection Reagent (Thermo Fisher Scientific) for siRNA. To induce ER stress apoptosis, cells were treated with 5 μM Tg (Calbiochem) or 10 μg/mL Tm (Calbiochem) for the indicated time periods unless otherwise stated.

Antibodies and Other Reagents. The following primary antibodies were used: anti-ubiquitin, anti-Myc, and anti-BiP/GRP78 (Santa Cruz Biotechnology); antibodies against PARP and Bcl-xL (Cell Signaling Technology); anti–β-tubulin, anti-Flag, and anti-HA antibodies (Sigma); antibody against calnexin, cytochrome C, and GM130 (BD Biosciences); and GFP, GAPDH, and Tim23 antibodies (Proteintech Group). The secondary antibodies were horseradish peroxidase (HRP) conjugated goat anti-rabbit/mouse IgG (H+L) (KPL), HRP-conjugated goat anti-mouse Fc fragment (Thermo Fisher Scientific), HRP-conjugated goat anti-rabbit Fc fragment (Jackson Immuno Research Laboratories), and Alexa Fluor 568 goat anti-rabbit or anti-mouse IgG (H+L) (Thermo Fisher Scientific). All other chemicals and reagents were from Sigma-Aldrich unless otherwise stated.

Construction of Expression Plasmids. Full-length cDNAs of human RNF183, Bcl-xL, and other Bcl-2 family members (Bcl-2s: Bcl-2, BAX, and BAD) were amplified from the cDNA library of HeLa cells or 293T cells by RT-PCR. The PCR product of wild-type or mutated RNF183/Bcl-xL/Bcl-2s was digested by EcoRI and SalI and subsequently cloned into a series of pCI-neo vectors (Promega) constructed with the following tags generated by our laboratory: Flag (Flag epitope at N or C terminus), 2xHA (HA epitope at C terminus), and GFP (GFP at N terminus).

Wild-type Ub and its lysine to arginine mutants (K29R, K48R, and K63R) were all constructed with pCI-neo vector via EcoRI and XbaI sites harboring Myc tag or HA tag.

GST-fusion RNF183 and its mutant were constructed by inserting a Myc tag at the N terminus of RNF183 into pGEX-6P-1. Bcl-2 and Bcl-xL were also constructed into pGEX-6P-1, but with an HA tag at the N terminus. Ub, UBA1, and UBCU5C expression plasmids were a kind gift from Ronggui Hu, Institute of Biochemistry and Cell Biology, Shanghai Institutes for Biological Sciences, CAS, Shanghai, China. Proteins were purified under native conditions using glutathione-Sepharose 4B (GE Healthcare Life Sciences) or Ni-NTA agarose (Qiagen) according to the manufacturer's instructions. All constructs were verified by sequencing.

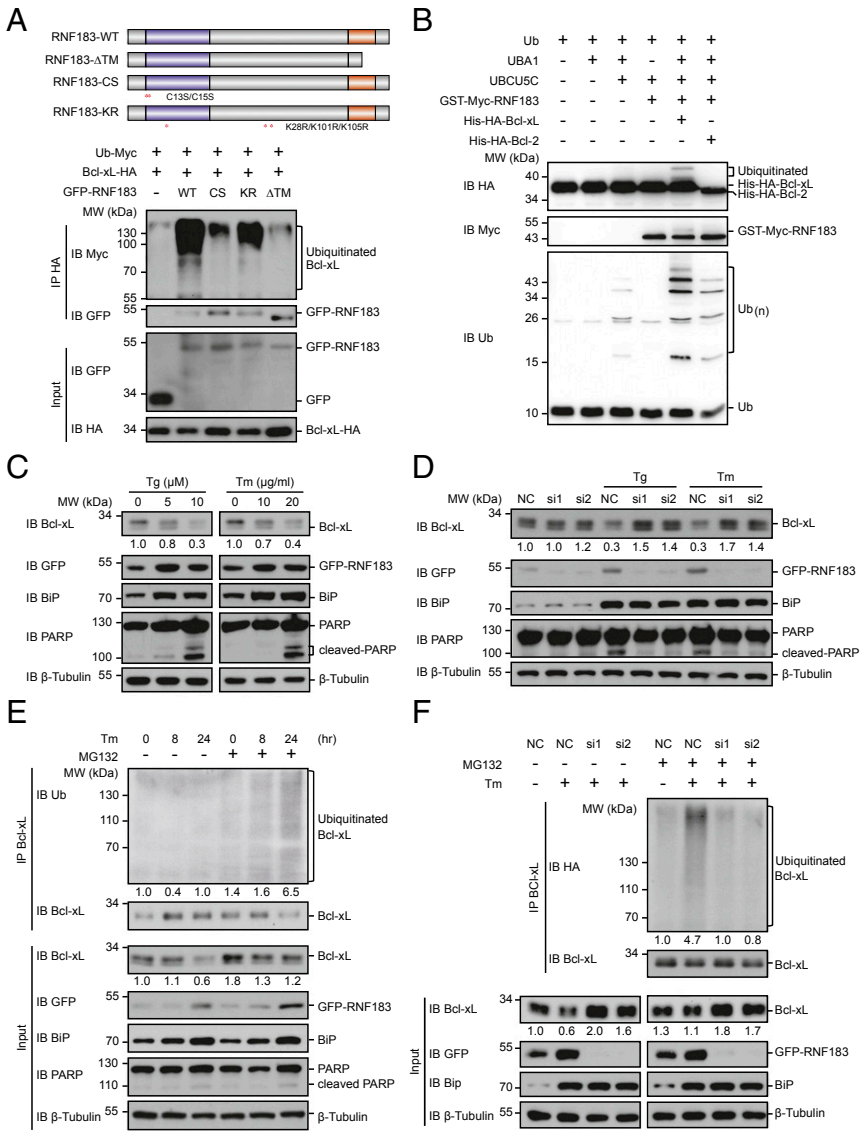

Fig. 7. RNF183 ubiquitinates Bcl-xL for degradation. (*A*) HeLa cells were cotransfected with Ub-myc, Bcl-xL-2xHA, and GFP-RNF183 as indicated. The *Top* shows the schematic diagram of RNF183 constructs used. The red asterisks (*) indicate the mutated amino acids in the RNF183 mutants. Cell lysates were precipitated with anti-HA antibody and IB carried out with the indicated antibodies. (*B*) Purified recombinant His-HA-Bcl-xL or His-HA-Bcl-2 was incubated with GST-Myc-RNF183 for the in vitro ubiquitination assay as described above. (*C*) KI-A6-HeLa cells were treated with Tg or Tm at the indicated concentrations. Endogenous levels of Bcl-xL, RNF183, PARP, and β-tubulin were analyzed by IB. Relative Bcl-xL expression levels are shown. (*D*) KI-A6-HeLa cells were transfected with indicated siRNAs, followed by Tg or Tm treatment for 24 h. Cell lysates were subjected to IB with Bcl-xL, GFP, PARP, and β-tubulin antibodies. Relative Bcl-xL protein level is shown. Relative Bcl-xL expression levels are shown. (*E*) KI-A6-HeLa cells were treated with Tm and proteasome inhibitor MG132 as indicated. Endogenous Bcl-xL was precipitated by anti-Bcl-xL antibodies under denaturing condition; the ubiquitination levels of Bcl-xL were analyzed by anti-Ub IB. Endogenous levels of Bcl-xL, RNF183, BiP, PARP, and β-tubulin were also analyzed by IB. Relative ubiquitination and Bcl-xL levels are shown. (*F*) As in *E*, but with treatment of control siRNA or siRNAs against RNF183.

CRISPR-Mediated Gene Targeting. The px260a-m2 and knockin vector pAAV-eGFP-C1 were gifts from Liu Pingsheng, Institute of Biophysics, CAS, Beijing, China. GFP-RNF183 knockin HeLa cells were generated following a similar procedure as described previously (37). The guide RNA (gRNA) sequences for human RNF183 (forward 5′-CAC CCC GCG AGC CTC CCC GTG TG-3′ and reverse 5′-AAA CCA CAC GGG GAG GCT TCG CGG C-3′) were ligated into the BbsI sites of px260a-m2. pAAV-GFP-RNF183 targeting vectors were constructed by the insertion of a left homologous arm (~1-kb genomic DNA sequence upstream of the ATG region of RNF183) and right homologous arm (~1-kb genomic DNA sequence downstream of ATG region of RNF183) into the pKI-eGFP-C1 vector. The two plasmids were cotransfected into HeLa cells and GFP-expressing clonal cell lines, isolated using FACS (BD Biosciences, Influx) 15 d after transfection. Genomic DNA containing insert GFP were amplified by PCR using the following primers and verified by sequencing: KF, 5′-AGC ACA AGG ATG GGA CTT -3′ and KR, 5′-TTA ATG AAT ACA GAA CAC-3′.

Reverse Transcription-PCR. Total RNA was isolated using TRIzol reagent (Thermo Fisher Scientific) according to the manufacturer's protocol. Reverse transcription was carried out with 1 μg RNA and oligo dT using reverse transcriptase (Promega). The cDNA products were subjected to 30 cycles of PCR using the human RNF183-specific forward primer 5′-GTG TCT ACG CCC ATC CT CAT-3′ and reverse primer 5′-CAC ACC CCA AAG GAA CTG CT-3′. GAPDH was amplified using primers 5′-CCA GGG CTG CTT TTA ACT C-3′ and 5′-TGG AAG ATG GTG ATG GGA TT-3′ as an internal control. Quantitative PCR (qPCR) amplifications were performed with 40 cycles using PowerUp SYBR Green Master Mix (Applied Biosystems) on a ABI-7300 real-time PCR machine (Applied Biosystems). Mature miR-7 expression levels were analyzed by miDETECT A TrackTM kit (RiboBio).

Immunofluorescent Microscopy. COS-7 cells cultured on the coverslips of 35-mm confocal dishes were washed with PBS three times and fixed with 4% paraformaldehyde in PBS for 15 min at room temperature. After washing

CELL BIOLOGY

with PBS, the cells were permeabilized with permeabilization buffer (eBioscience) for 10 min, washed again with PBS, and blocked with 5% goat serum in PBS for 1 h at room temperature. The cells were then incubated with primary antibodies in a humidity chamber at 37 °C for half an hour. As a negative control, cells were labeled with rabbit IgG or mouse IgG. After washing four times with PBS, the cells were incubated with secondary antibodies diluted in PBS for 20 min at room temperature and washed again four times. The cells were imaged using an Olympus LSCMFV1200 confocal microscope.

Cell Viability Assay. Cell viability was evaluated using the MTT [3-(4, 5-dimethylthiazol-2-yl)-2, 5-diphenyltetrazolium bromide] reduction conversion assay. Briefly, HeLa cells were plated at 2×10^4 cells per well in 96-well tissue culture plates 24 h before transfection. The cells were then transfected with the indicated plasmid. At 24 h posttransfection, 0.5 mg/mL MTT was added to the wells and incubated at 37 °C for 4 h. The formazan product was dissolved in dimethyl formamide and read at 570 nm using a microplate reader (VICTOR3, Perkin-Elmer). The percentage of viable cells was calculated by considering the untreated samples as 100%.

Annexin V Staining. HeLa cells were treated as described in the figure legends and trypsinized for 1 min using 0.1% trypsin at 37 °C, washed twice with ice-cold PBS, and resuspended in 1× binding buffer at a concentration of 1×10^6 cells per milliliter. A total of 100 μL cells were incubated with Alexa Fluor-488 Annexin V and propidium iodide (Thermo Fisher Scientific) for 15 min on ice. Before analysis, 300 μL binding buffer was added and analyzed on a FACS Calibur flow cytometer (BD Biosciences). For microscopy, HeLa cells cultured on the coverslips were stained with PE-Annexin V (eBioscience) for 15 min and images acquired with a fluorescence microscope (Olympus LSCMFV1200).

Western Blotting. Cells were washed once in ice-cold PBS and lysed in whole cell lysis buffer [50 mM Tris·HCl (pH 7.5), 150 mM NaCl, 1 mM EDTA, 1% Triton X-100, 0.1% SDS, 10% glycerol, and 1× protease inhibitor mixture (Roche)] on ice for 15 min. The precipitated samples were resolved by SDS/PAGE electrophoresis and transferred to a PVDF membrane (Millipore). The membrane was probed with the indicated primary antibody overnight at 4 °C after blocking with 5% BSA in Tris-buffered saline supplemented with 0.1% Tween 20 (TBS-T), followed by incubation with an appropriate secondary HRP-conjugated antibody for 1 h at room temperature and washing with TBS-T. Signals were detected using an enhanced chemiluminescence kit (ECL, GE Healthcare Life Sciences).

Band densities were quantified using Gel-Pro Analyzer version 4.0 (Media Cybernetics).

Subcellular Fractionation. Subcellular fractionation was performed as described (38). Briefly, KI-A6 HeLa cells were washed with ice-cold PBS, subsequently suspended in Buffer A (Tricine 20 mM, sucrose 250 mM, pH 7.8, and 1× protease inhibitor mixture), and kept on ice for 20 min. The cells were homogenized before centrifugation at 3,000 × *g* for 10 min to remove the nucleus. The supernatant was considered the postnuclear supernatant (PNS). The PNS was loaded on 30% Percoll and centrifuged at 29,000 rpm for 30 min in a Beckman SW41 Ti rotor. Fractionated samples were collected from top to bottom in 1,000-μL fractions and subjected to SDS/PAGE and Western blotting with different antibodies.

The HeLa PNS was further centrifuged at 100,000 × *g* (100.3 rotor; Beckman) for 40 min at 4 °C to obtain the cytosol and total membrane of all organelles.

For the alkaline extraction assay, the total membrane fraction prepared from KI-A6 HeLa cells was subjected to alkaline extraction (0.1 M Na_2CO_3, pH 11) followed by centrifugation at 100,000 × *g* for 40 min. Both the pellets and the supernatant soluble fractions were subjected to immunoblotting.

For the proteinase K protection assay, total membrane prepared from KI-A6-HeLa cells was incubated in concentration gradients of proteinase K for 5 min with/without 1% Triton X-100 (vol/vol) at room temperature. The digestion reaction was stopped immediately by adding 1 μM PMSF. Samples were prepared for Western blotting.

Immunoprecipitation and GST Pull-Down Assay. For immunoprecipitation, HeLa cells were lysed on ice in IP buffer (50 mM Tris·HCl, 150 mM NaCl, 1 mM EDTA, 1% Triton-X 100, 10% glycerol, and 1× protease inhibitor mixture, pH 7.5). The clarified cell lysate was incubated with 1–2 μg primary antibody at 4 °C for 2 h. Next, 20 μL of Protein A/G PLUS-Agarose (Santa Cruz Biotechnology) was added and incubated with protein lysate for another 2 h at 4 °C. The precipitates were collected by centrifugation, washed four times with IP lysis buffer, and analyzed by Western blotting as described above.

For the GST pull-down assay, 10 μg purified GST-Myc-RNF183 or RNF183 mutants were incubated with 10 μg His-Bcl-xL or its mutant in 500 μL IP buffer at 4 °C for 2 h. GST-myc was used as a negative control. Glutathione-Sepharose 4B (20 μL; GE Healthcare Life Sciences) was added and incubated for another 2 h at 4 °C. The resins were washed four times with IP buffer and the bound proteins mixed with SDS/PAGE sample buffer and analyzed by immunoblotting with appropriate antibodies.

In Vivo and in Vitro Ubiquitination Assay. For the in vivo ubiquitination assay, HeLa cells seeded in 60-mm culture dishes were transiently cotransfected with the indicated plasmids. At 24 h posttransfection, cells were treated with 10 μM MG132 (Merck Calbiochem) for 4 h before harvest. Cells were lysed in 1,000 μL IP buffer and the lysate was sonicated briefly on ice and clarified by centrifugation. The supernatants were subjected to immunoprecipitation with the indicated antibodies. Samples were separated by SDS/PAGE and immunoblotted with the indicated antibodies.

For ubiquitination assessed under denatured conditions, cells were homogenized in 100 μL denaturing lysis buffer (50 mM Tris·HCl, 150 mM NaCl, 1% SDS, 5 mM EDTA, 10 mM DTT, 15 units/mL DNaseI, 10 μM MG132, and protease inhibitor mixture, pH 7.5). Lysates were heated to 95 °C for 5 min and diluted with 0.9 mL IP lysis buffer. After sonication and centrifugation, the supernatants were subjected to immune precipitation with the indicated antibodies.

In vitro ubiquitination reactions were prepared and analyzed as described previously (39). Purified GST-RNF183 (1 μM) or His-tagged Bcl-xL (or Bcl-2) (1 μM) was incubated with UBA1 (110 nM), UbCH5C (4 μM), and Ub (20 μM) in a ubiquitination reaction buffer [25 mM Tris·HCl, 150 mM NaCl, 5 mM $MgCl_2$, 1 mM DTT, 0.1% (vol/vol) Triton X-100, 5 mM ATP, pH 7.5] to a final volume of 50 μL for 1 h at 37 °C. After the reaction, the total proteins generated in the ubiquitination reaction were analyzed by Western blotting.

RNA Interference. The target sequences of human RNF183 siRNA synthesized by Invitrogen were as follows: RNF183-si1, sense 5′-CCC UCA GUU CCG CAU CUU UTT-3′ and anti-sense 5′-AAA GAU GCG GAA CUG AGG GTT-3′; RNF183-si2, sense 5′-AAA AGA UGG AGA AUA UGA GCA-3′ and anti-sense 5′-CUC AUA UUC UCC AUC UUU UGG-3′; and Nc-si, sense 5′-UUC UCC GAA CGU GUC ACG UTT-3′ and anti-sense 5′-ACG UGA CAC GUU CGG AGA ATT-3′. Interference of RNF183 was analyzed by Western blotting.

Statistical Analysis. All data were analyzed using Prism 5 (GraphPad).

ACKNOWLEDGMENTS. We thank Drs. Ronggui Hu, Rongguang Zhang, and Pingsheng Liu for providing plasmids and materials; Drs. Peter Walter and Carmela Sidrauski for providing ISRIB; Dr. David Ron for providing 4μ8C; Drs. Baoliang Song and Yongjian Wang for technical help; Dr. Pedro Carvalho for critically reading the manuscript; and Dr. Alicia Prater for proofreading. J.H. is supported by the National Key Research and Development Program (Grant 2016YFA0500201), the National Natural Science Foundation of China (Grants 31225006 and 3142100024), and an International Early Career Scientist grant from Howard Hughes Medical Institute.

1. Hessa T, et al. (2011) Protein targeting and degradation are coupled for elimination of mislocalized proteins. *Nature* 475:394–397.
2. Smith MH, Ploegh HL, Weissman JS (2011) Road to ruin: Targeting proteins for degradation in the endoplasmic reticulum. *Science* 334:1086–1090.
3. Walter P, Ron D (2011) The unfolded protein response: From stress pathway to homeostatic regulation. *Science* 334:1081–1086.
4. Hetz C (2012) The unfolded protein response: Controlling cell fate decisions under ER stress and beyond. *Nat Rev Mol Cell Biol* 13:89–102.
5. Yoshida H, Matsui T, Yamamoto A, Okada T, Mori K (2001) XBP1 mRNA is induced by ATF6 and spliced by IRE1 in response to ER stress to produce a highly active transcription factor. *Cell* 107:881–891.
6. Calfon M, et al. (2002) IRE1 couples endoplasmic reticulum load to secretory capacity by processing the XBP-1 mRNA. *Nature* 415:92–96.
7. Harding HP, Zhang Y, Ron D (1999) Protein translation and folding are coupled by an endoplasmic-reticulum-resident kinase. *Nature* 397:271–274.
8. Harding HP, et al. (2000) Regulated translation initiation controls stress-induced gene expression in mammalian cells. *Mol Cell* 6:1099–1108.
9. Zinszner H, et al. (1998) CHOP is implicated in programmed cell death in response to impaired function of the endoplasmic reticulum. *Genes Dev* 12:982–995.
10. Haze K, Yoshida H, Yanagi H, Yura T, Mori K (1999) Mammalian transcription factor ATF6 is synthesized as a transmembrane protein and activated by proteolysis in response to endoplasmic reticulum stress. *Mol Biol Cell* 10:3787–3799.

11. Tabas I, Ron D (2011) Integrating the mechanisms of apoptosis induced by endoplasmic reticulum stress. *Nat Cell Biol* 13:184–190.
12. Hetz C, et al. (2006) Proapoptotic BAX and BAK modulate the unfolded protein response by a direct interaction with IRE1alpha. *Science* 312:572–576.
13. Reed JC (2006) Proapoptotic multidomain Bcl-2/Bax-family proteins: Mechanisms, physiological roles, and therapeutic opportunities. *Cell Death Differ* 13:1378–1386.
14. Puthalakath H, et al. (2007) ER stress triggers apoptosis by activating BH3-only protein Bim. *Cell* 129:1337–1349.
15. Urano F, et al. (2000) Coupling of stress in the ER to activation of JNK protein kinases by transmembrane protein kinase IRE1. *Science* 287:664–666.
16. Lu M, et al. (2014) Opposing unfolded-protein-response signals converge on death receptor 5 to control apoptosis. *Science* 345:98–101.
17. Upton JP, et al. (2012) IRE1α cleaves select microRNAs during ER stress to derepress translation of proapoptotic Caspase-2. *Science* 338:818–822.
18. Yachdav G, et al. (2014) PredictProtein–An open resource for online prediction of protein structural and functional features. *Nucleic Acids Res* 42:W337–W343.
19. Doudna JA, Charpentier E (2014) Genome editing. The new frontier of genome engineering with CRISPR-Cas9. *Science* 346:1258096.
20. Hsu PD, Lander ES, Zhang F (2014) Development and applications of CRISPR-Cas9 for genome engineering. *Cell* 157:1262–1278.
21. Sidrauski C, et al. (2013) Pharmacological brake-release of mRNA translation enhances cognitive memory. *eLife* 2:e00498.
22. Maurel M, Chevet E, Tavernier J, Gerlo S (2014) Getting RIDD of RNA: IRE1 in cell fate regulation. *Trends Biochem Sci* 39:245–254.
23. Deshaies RJ, Joazeiro CA (2009) RING domain E3 ubiquitin ligases. *Annu Rev Biochem* 78:399–434.
24. Maxfield KE, et al. (2015) Comprehensive functional characterization of cancer-testis antigens defines obligate participation in multiple hallmarks of cancer. *Nat Commun* 6:8840.
25. Yu Q, et al. (2016) E3 ubiquitin ligase RNF183 is a novel regulator in inflammatory bowel disease. *J Crohn's Colitis* 10:713–725.
26. Ikeda F, Dikic I (2008) Atypical ubiquitin chains: New molecular signals. 'Protein Modifications: Beyond the Usual Suspects' review series. *EMBO Rep* 9:536–542.
27. Lerner AG, et al. (2012) IRE1α induces thioredoxin-interacting protein to activate the NLRP3 inflammasome and promote programmed cell death under irremediable ER stress. *Cell Metab* 16:250–264.
28. Lin JH, et al. (2007) IRE1 signaling affects cell fate during the unfolded protein response. *Science* 318:944–949.
29. White C, et al. (2005) The endoplasmic reticulum gateway to apoptosis by Bcl-X(L) modulation of the InsP3R. *Nat Cell Biol* 7:1021–1028.
30. Eno CO, et al. (2012) Distinct roles of mitochondria- and ER-localized Bcl-xL in apoptosis resistance and Ca2+ homeostasis. *Mol Biol Cell* 23:2605–2618.
31. Csordás G, et al. (2006) Structural and functional features and significance of the physical linkage between ER and mitochondria. *J Cell Biol* 174:915–921.
32. Rowland AA, Voeltz GK (2012) Endoplasmic reticulum-mitochondria contacts: Function of the junction. *Nat Rev Mol Cell Biol* 13:607–625.
33. Metzger MB, Maurer MJ, Dancy BM, Michaelis S (2008) Degradation of a cytosolic protein requires endoplasmic reticulum-associated degradation machinery. *J Biol Chem* 283:32302–32316.
34. Wang X, Li S, Wang H, Shui W, Hu J (2017) Quantitative proteomics reveal proteins enriched in tubular endoplasmic reticulum of *Saccharomyces cerevisiae*. *eLife* 6: e23816.
35. Llambi F, et al. (2016) BOK is a non-canonical BCL-2 family effector of apoptosis regulated by ER-associated degradation. *Cell* 165:421–433.
36. Geng R, et al. (2017) RNF183 promotes proliferation and metastasis of colorectal cancer cells via activation of NF-κB-IL-8 axis. *Cell Death Dis* 8:e2994.
37. Schumann K, et al. (2015) Generation of knock-in primary human T cells using Cas9 ribonucleoproteins. *Proc Natl Acad Sci USA* 112:10437–10442.
38. Wang QC, et al. (2016) TMCO1 is an ER Ca(2+) load-activated Ca(2+) channel. *Cell* 165: 1454–1466.
39. Liu Z, et al. (2014) Ubiquitylation of autophagy receptor Optineurin by HACE1 activates selective autophagy for tumor suppression. *Cancer Cell* 26:106–120.